MECHANISM FOR THE UPCONVERSION PROCESS FOR $Y_2O_3:Er^{3+},Yb^{3+}$ PHOSPHORS

Liviu DUDAS[1], Daniela BERGER[2], Cristian MATEI[3]

Yttria ceramic as host matrix for different ratio of Er^{3+} as activator and Yb^{3+} as sensitizer were obtained through coprecipitation method followed by powders pressing and sintering at 1300°C for 4h. The upconversion photoluminescence spectra were recorded after the ceramic irradiation at 976 nm. The energy levels involved in the emission in the visible range and a mechanism for upconversion process was proposed.

Keywords: Er^{3+},Yb^{3+} co-doped Y_2O_3, coprecipitation, hydrothermal treatment, upconversion mechanism, photoluminescence spectra, Stark splitting

1. Introduction

Upconverting materials are optical materials containing rare earth (RE) ions, which can convert the incident excitation radiation from the infrared range to the visible or ultraviolet range. The photoluminescence (PL) properties depend on both the type of host matrix and the nature and concentration of luminescent centers (RE dopant ions) [1-4]. The upconverting materials have various applications from biomedicine to harvesting solar energy [5]. Another application is the phosphor thermometry based on the temperature-dependent lifetime of emission lines of the RE ions, a promising technique that can be used as non-contact remote temperature sensing in a corrosive environment or in large furnaces [6]. Recently, Yang et al. reported that Eu (1% mol) and Er (0.5-5% mol) co-doped yttria-stabilized zirconia could be used as dual-sensor for simultaneous measurements of oxygen partial pressure and temperature up to 600 °C [7].

Yttria, as a host matrix for Er^{3+} and Yb^{3+} ions as an activator-sensitizer pair, was extensively studied for the upconversion process of incident NIR irradiation [8-12]. Herein, we report the obtaining and characterization of Er, Yb co-doped yttria phosphors. From the literature, it is not very clear the mechanism of the

[1] PhD Student, Department of Inorganic Chemistry, Physical-Chemistry & Electrochemistry, National University for Science and Technology POLITEHNICA of Bucharest, Romania, e-mail: liviu_dudas@yahoo.com

[2] Prof, Department of Inorganic Chemistry, Physical-Chemistry & Electrochemistry, National University for Science and Technology POLITEHNICA of Bucharest, Romania, e-mail: daniela.berger@upb.ro, daniela.berger@unstpb.ro

[3] Prof, Department of Inorganic Chemistry, Physical-Chemistry & Electrochemistry, National University for Science and Technology POLITEHNICA of Bucharest, Romania, e-mail: cristian.matei@upb.ro, cristian.matei@unstpb.ro

energy transfer between the dopant ions and the upconversion of NIR photons by Er^{3+} when sensitized by Yb^{3+} and an in-depth analysis must be done to understand this process. This work is an attempt to underline some details in this regard.

2. Experimental

2.1 Obtaining of the Er,Yb co-doped yttria ceramics

Yttrium, erbium and ytterbium nitrates ($Y(NO_3)_3 \cdot 6H_2O$, $Er(NO_3)_3 \cdot 5H_2O$ and $Yb(NO_3)_3 \cdot 5H_2O$, 99.9%) and sodium hydroxide from Sigma-Aldrich were used as received. 0.1M stock aqueous solutions of metallic nitrates were prepared and used for the synthesis of Er,Yb co-doped yttria powders: Y_2O_3:Er1% (denoted as YO1-0), Y_2O_3:Er1%,Yb2% (YO1-2), Y_2O_3:Er1%,Yb4% (YO1-4), and Y_2O_3:Er1%,Yb8% (YO1-8).

In the case of the hydrothermal method, the precipitation agent was a 5M aqueous solution of NaOH which was added dropwise to the solutions containing the metallic nitrates mixed in the appropriate molar ratios, under constant magnetic stirring, until pH 14. Firstly, the reaction mixtures were aged at 60 °C overnight and then a hydrothermal treatment at 160 °C for 24 h was applied. The resulting precipitates were filtered off and washed intensively with water until neutral pH, dried and calcined at 500 °C for 3 h.

The second route applied for obtaining Er, Yb co-doped yttria powders was the coprecipitation method. Thus, to the 0.1 M aqueous solution of metallic nitrates mixed in the desired molar ratios, 10 M aqueous NaOH solution was dropped under magnetic stirring. The reaction mixture having pH 14 was aged under magnetic stirring, at 60 °C for 20 h. The resulting white precipitate was filtered off, washed with water, dried at 110 °C, and calcinated at 800 °C for 3 h.

Er, Yb co-doped yttria ceramic pellets with 13mm diameter and 2mm thickness were obtained from the calcinated powders through uniaxial pressing at 100 bar for 1 minute and sintering them at 1300 °C for 4 h.

2.2 The characterization of the RE co-doped yttria samples

Before and after the calcination step, the powders were characterized by powder X-ray diffraction (XRD) (Rigaku Miniflex II, Cu K_α radiation in 2θ range of 10°–70°, with 2°/min rate) and scanning electron microscopy (SEM) (Tescan Vega 3LM). The sintered ceramic pellets were also characterized by XRD and SEM.

2.3 The measurement of the photoluminescence spectra

The ceramic pellets were illuminated with a laser diode (LCU98E042Ap) of 976nm wavelength focused with a standard low-power laser collimator. The diode was supplied with 202 mA, which, according to the datasheet of the diode,

the NIR light emitted power is around 45 mW at 30 °C. The PL spectra in the visible range were measured with an HR4000CG-UV-NIR spectrometer from Ocean Optics, using the OceanView software version 1.6.7. The diameter of the illuminated area was 0.5 mm and the distance of the optical fiber head entrance to the illuminated area was 3 mm. The diameter of the optical fiber input was 200 μm (Fig. 1). Sampling time was 40 ms and the average made over 1500 samples for a total measurement duration of 60 s for a single spectrum.

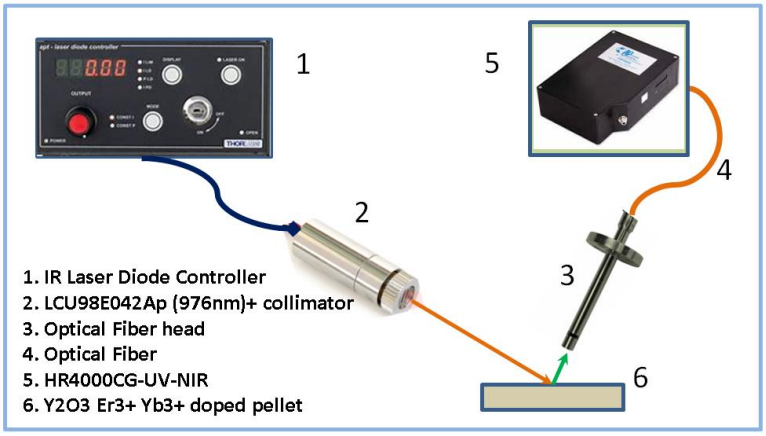

Fig. 1-Setup for the upconversion PL spectra measurement.

3. Results and discussion

3.1 The Characterization of the Er, Yb co-doped yttria samples

The SEM investigation of the samples obtained by the hydrothermal method before the calcination at 500 °C showed the formation of acicular and tubular crystals with an average of 1 μm diameter and 10 μm length (Fig. 2) and the XRD patterns proved the formation of the crystalline metallic hydroxides (data not shown). After the calcination at 500 °C for 3 h, the yttria phase with cubic symmetry and a secondary phase of Er_2O_3 were identified in the XRD patterns (Fig. 3 - upper pattern, cyan), which is an indication that the hydrothermal treatment led to the segregation of Er_2O_3, the cause being the lower energy of formation of $Er(OH)_3$ than that of $Y(OH)_3$. Regarding the morphology of the RE-doped Y_2O_3 crystals obtained after the calcination at 500 °C, one can notice the cracks of the tubular rods due to the loss of the hydroxyl groups (Fig. 2 C and D).

The segregation of the RE oxide phases compelled us to abandon the hydrothermal method and synthesize the oxide powders through the coprecipitation route. The coprecipitation route led to the formation of oxide powders with a different morphology than that in the case of the hydrothermal method. As the SEM

characterization revealed, the YO1-4 powder have unregular, submicron, aggregated particles (Fig. 4).

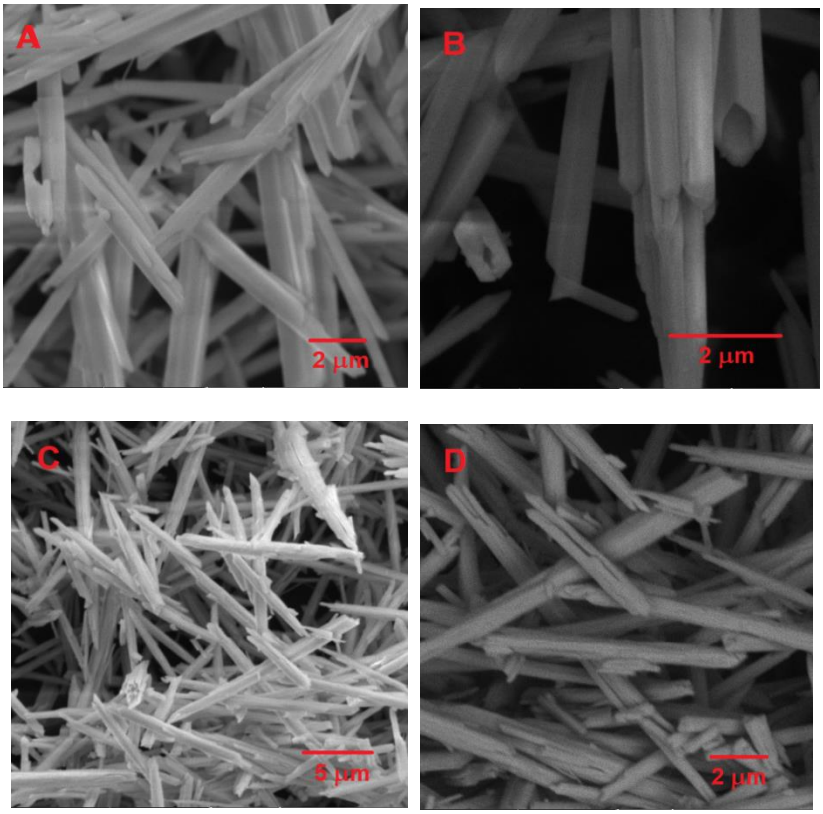

Fig. 2 - SEM images of $Y(OH)_3$:Er1%,Yb4% obtained by hydrothermal treatment at 160 °C (A, B) and Y_2O_3:Er1%,Yb4% crystals after the hydroxides calcination at 500 °C for 3 h (C, D).

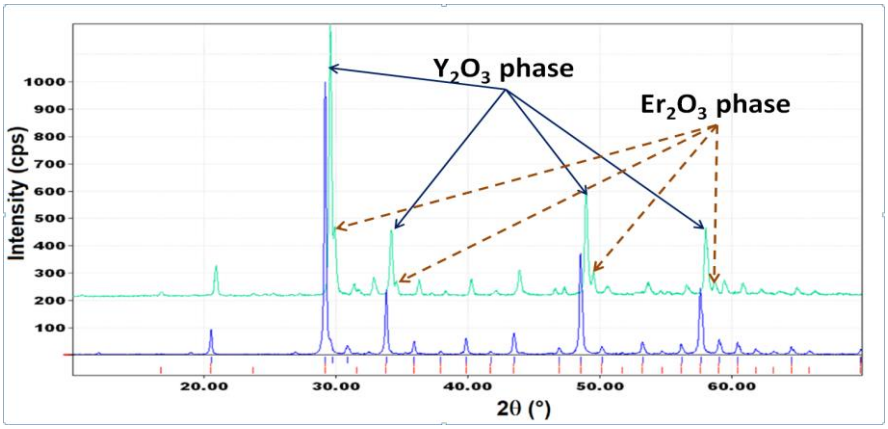

Fig. 3 - XRD patterns for YO1-2 powders: Cyan pattern (up): XRD after the hydrothermal treatment at 160 °C-24h and calcination at 500 °C-3h; Blue pattern (low): XRD resulted after the coprecipitation method; (bottom marks: ICCD 96-100-9045)

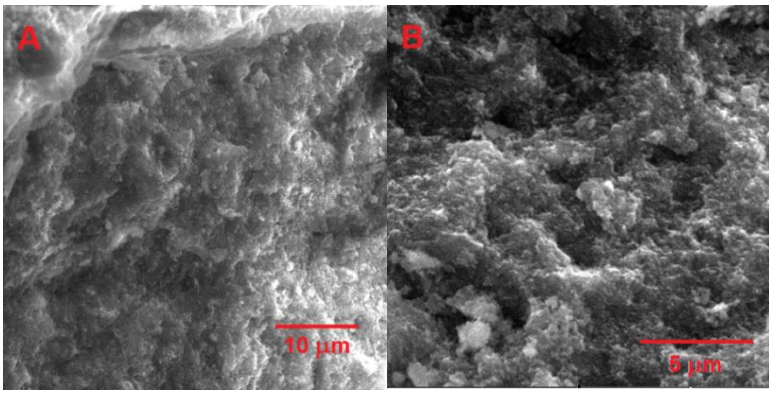

Fig. 4 – SEM images for the case of YO1-4 powder obtained by coprecipitation after calcination at 800 °C.

The XRD patterns of all Er,Yb co-doped yttria samples (example in Fig. 5) proved the formation of a single cubic symmetry crystalline phase, meaning that the Er^{3+} and Yb^{3+} doping ions are well accommodated by the yttria host matrix neither segregating nor introducing defects. The SEM investigation of the YO1-4 pellet which can be seen in Fig. 6, reveals a porous ceramic microstructure consisting of rounded convex grains of 250-350 nm diameter and pores of around 100 nm diameter.

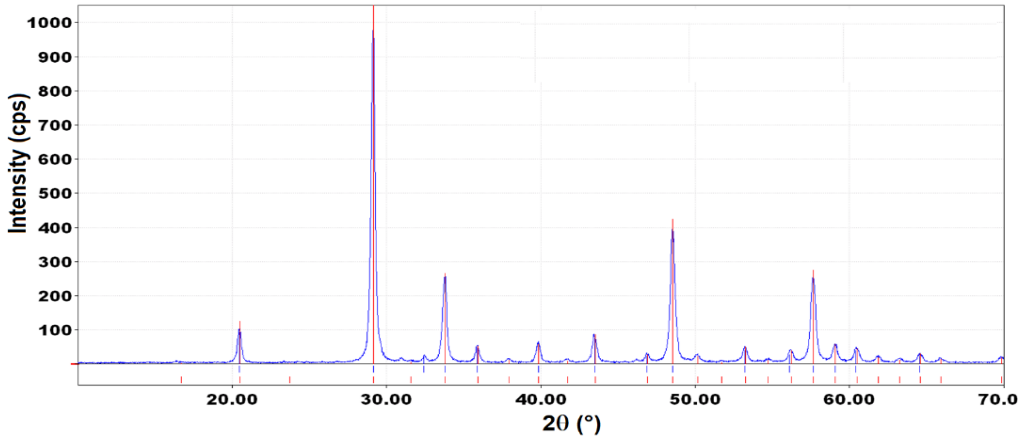

Fig. 5 - XRD for YO1-4 ceramic resulted from powders obtained by the coprecipitation method (bottom marks: ICCD 96-100-9045). No additional phases are observed.

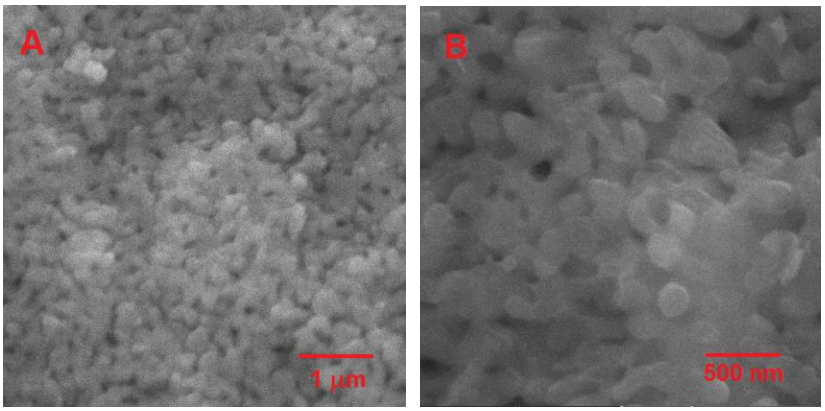

Fig. 6 - SEM images for the case of YO1-4 ceramic pellet sintered at 1300°C and obtained from powders prepared by coprecipitation method.

3.2. The upconversion spectra of the Er, Yb co-doped yttria ceramics

The photoluminescence (PL) spectra of Y_2O_3:Er,Yb phosphors, presented in Figs. 7-10, reveal a crystal field that is sufficiently strong to lift the degeneracy of the energy levels of Er^{3+} which are involved in the upconversion process and, by that, resolving their sub-structure. The spectra with the highest intensities for each emission transition were chosen for the peak fitting.

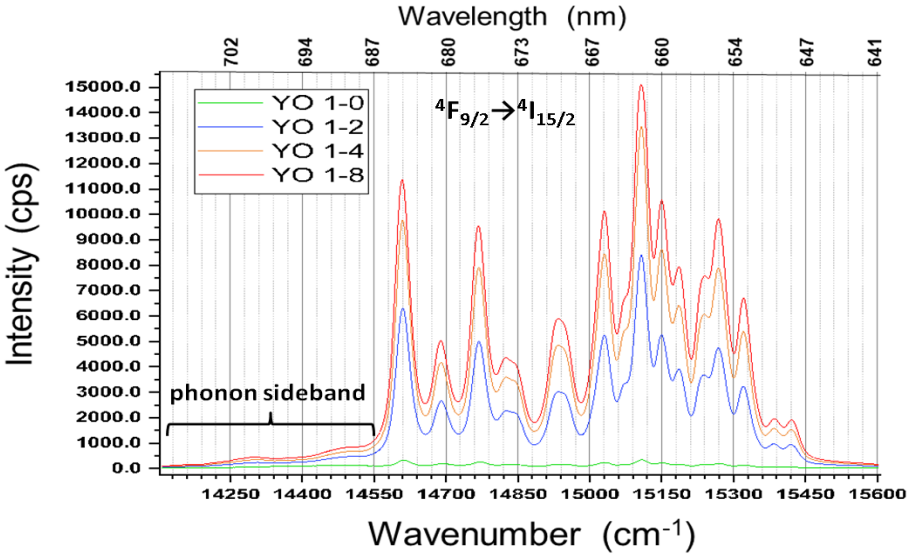

Fig. 7 – PL spectra of Y_2O_3:Er,Yb ceramics for $^4F_{9/2}\rightarrow{}^4I_{15/2}$ (red) transition of Er^{3+}.

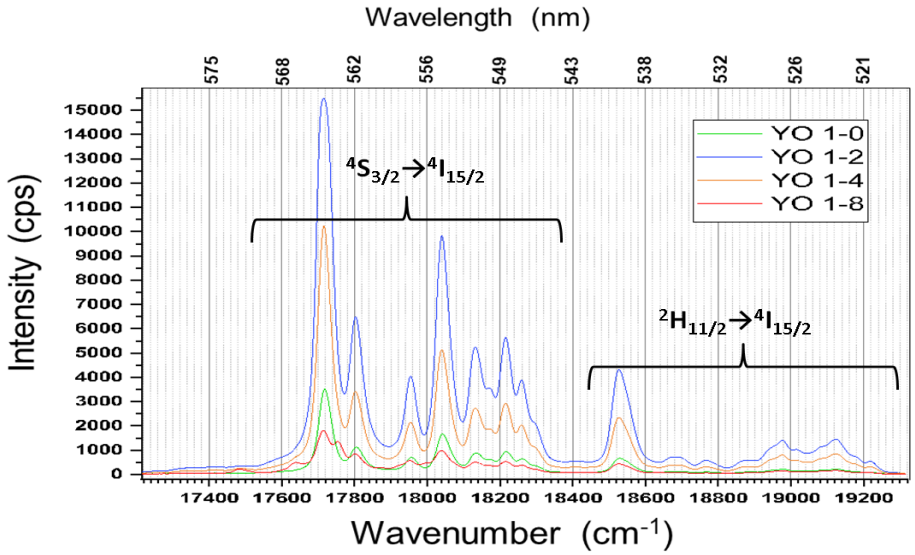

Fig. 8 – PL spectra of Y_2O_3:Er,Yb ceramics for $^4S_{3/2}\rightarrow{}^4I_{15/2}$ and $^2H_{11/2}\rightarrow{}^4I_{15/2}$ (green) transitions of Er^{3+}.

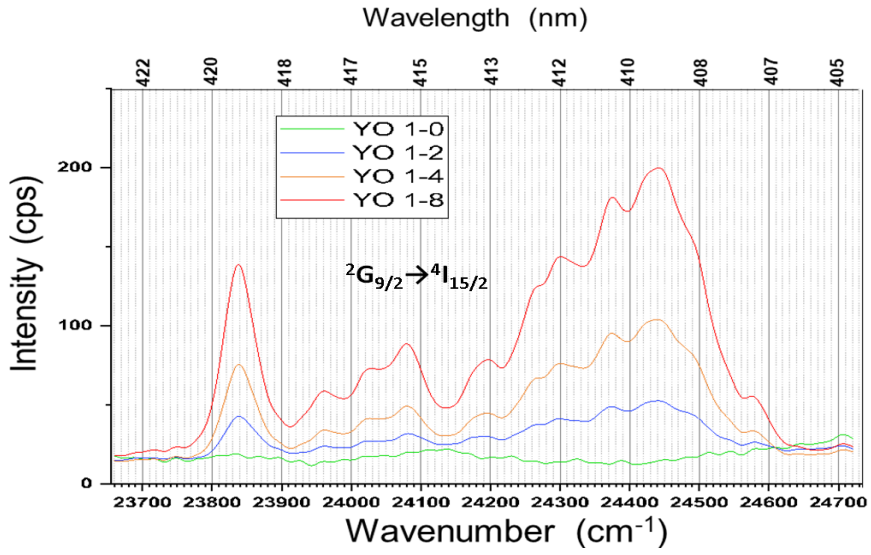

Fig. 9 – PL spectra of Y_2O_3:Er,Yb ceramics for $^2G_{9/2}\rightarrow{}^4I_{15/2}$ (blue) transition of Er^{3+}.

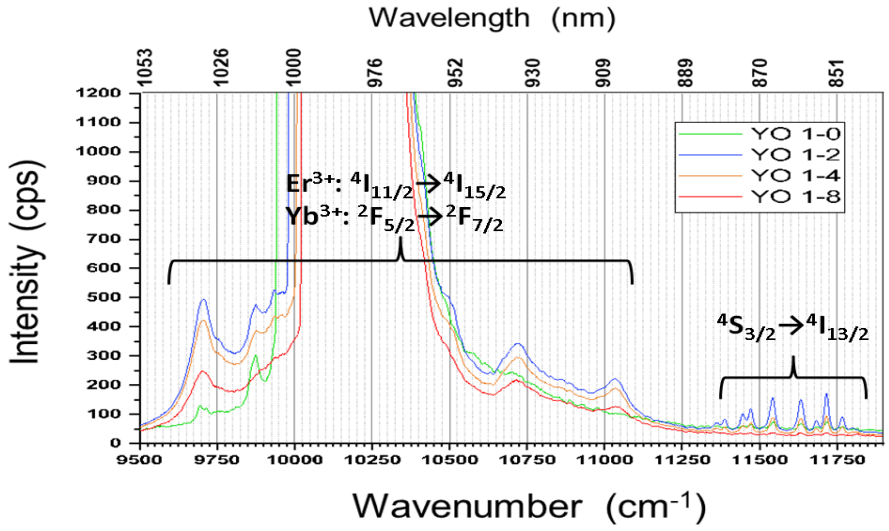

Fig. 10 - PL spectra for all obtained Y_2O_3:Er,Yb ceramics. Observe the bands corresponding to the $^4S_{3/2}\rightarrow{}^4I_{13/2}$ transition in the range of 11400 - 11800 cm^{-1} (862nm). The saturation zone is due to the reflection of the incident irradiation of 976 nm and the cumulated intensities of $^4I_{11/2}\rightarrow{}^4I_{15/2}$ transition of Er^{3+} and $^2F_{5/2}\rightarrow{}^2F_{7/2}$ of Yb^{3+}.

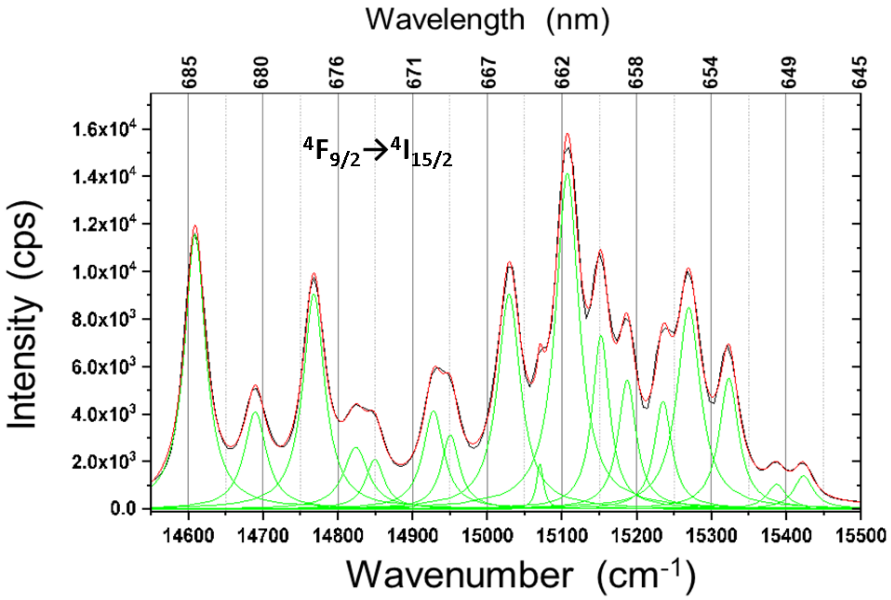

Fig. 11 - Fitted PL spectrum for $^4F_{9/2}\rightarrow{}^4I_{15/2}$ transition of Er^{3+} in the YO1-8 case.

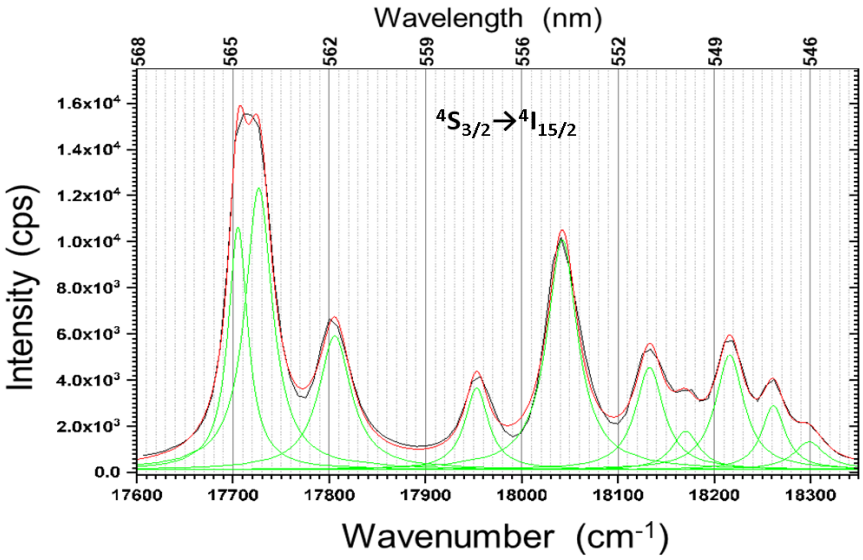

Fig. 12 - Fitted PL spectrum for $^4S_{3/2}\rightarrow{}^4I_{15/2}$ transition of Er^{3+} in the YO1-2 case.

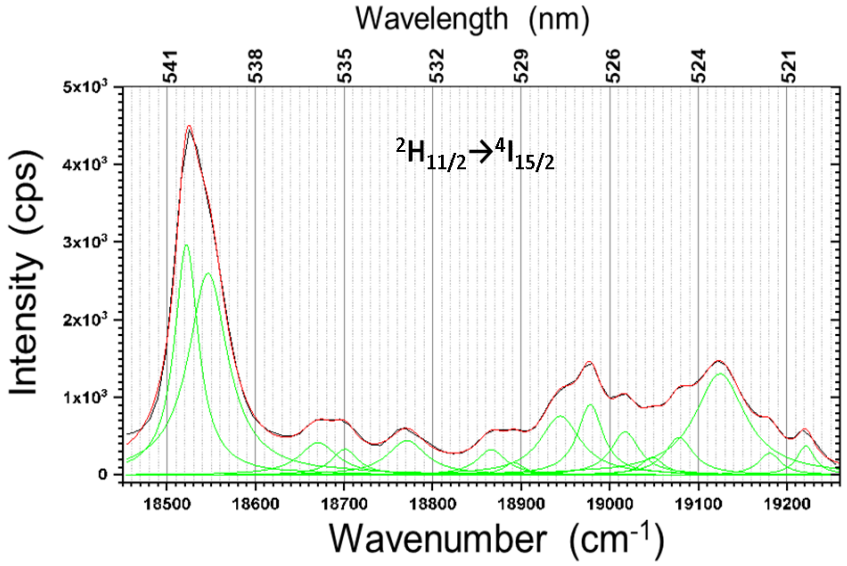

Fig. 13 - Fitted PL spectrum for $^2H_{11/2}\rightarrow{}^4I_{15/2}$ transition of Er^{3+} in the YO1-2 case.

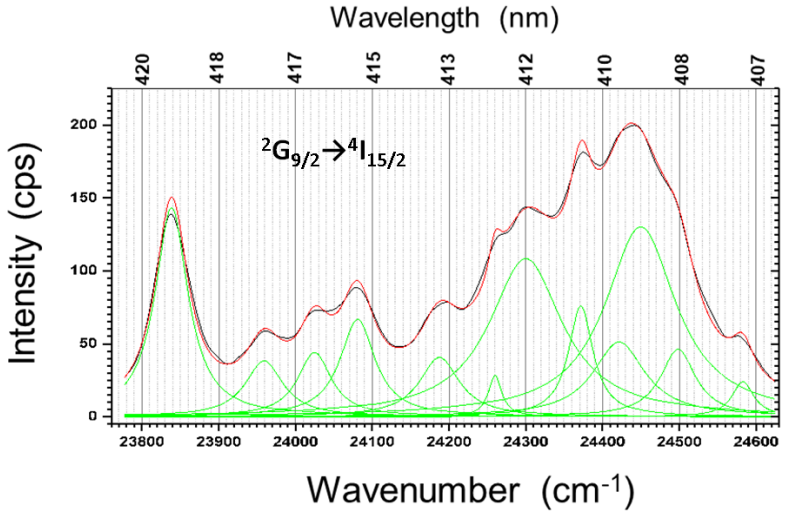

Fig. 14 - Fitted PL spectrum for $^2G_{9/2} \rightarrow {}^4I_{15/2}$ transition of Er^{3+} in the YO1-8 case.

The thermal populating of $^2H_{11/2}$ is observed, and the relative intensities comparison of the $^2H_{11/2}\rightarrow{}^4I_{15/2}$ and $^4S_{3/2}\rightarrow{}^4I_{15/2}$ emissions indicate a local temperature of the illuminated area of around 57 °C. The temperature was calculated with the equation (15) from [13].

There is a weak signature of three photons upconversion process, which corresponds to the $^2G_{9/2}\rightarrow{}^4I_{15/2}$ transition at 415nm. In the infrared part, the spectra show also a weak signal around 862nm (11400-11800 cm^{-1}) that corresponds to the $^4S_{3/2}\rightarrow{}^4I_{13/2}$ transition. The phonon sideband is uniform only in the case in which Er^{3+} ions were not sensitized by Yb^{3+} ions (Fig. 15 - curve at bottom):

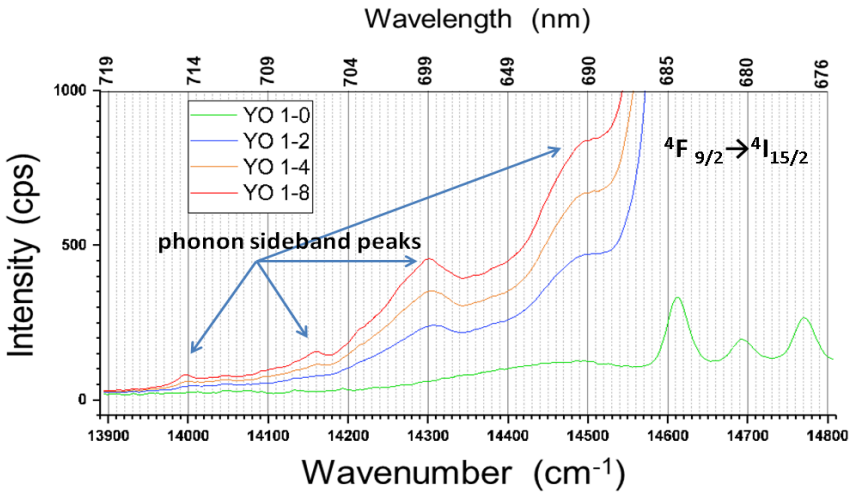

Fig. 15 - Phonon sidebands in PL spectra of YO1-0, YO1-2, YO1-4, and YO1-8 in the case of the emission in red ($^4F_{9/2}\rightarrow{}^4I_{15/2}$ transition). Observe the uniformity in the case of Er^{3+} only (green curve at bottom) and the superposition peaks when Yb^{3+} ions are present.

While for the ceramics containing 2%, 4%, and 8% of Yb^{3+} dopant concentrations, four superposition peaks can be observed, which shows that the presence of Yb^{3+} ions significantly changes the phonon dispersion, promoting some preferential directions in the crystal lattice.

3.3. The energy levels of the yttria embedded Er^{3+} ion

The PL spectra which were most intense for each wavelength range, were chosen for fitting and the resulting curves are presented in Figs. 11-14. The fitting process was accurate, showing a close superposition of the measured data (black) with the individual peaks sum (red). Table 1 presents the resulting emission lines with their center and areas (all Lorentzian). The variety of widths and heights of the peaks is an indication of the complex structure of wavefunctions for the energy levels and the transitions between them. The lines that have a higher relative area show that certain $LSJM_J$ quantum numbers are favored in the composition of each level wavefunction.

The line centers (Table 1) were used to approximate the energy of the individual Stark sublevels involved in the transitions [14-18].

Table 1

Centers (cm^{-1}) of the emission lines resulted from the fitting process of the representative PL spectra. Areas of the peaks are also shown.

$^4F_{9/2} \rightarrow {}^4I_{15/2}$		$^4S_{3/2} \rightarrow {}^4I_{15/2}$		$^2H_{11/2} \rightarrow {}^4I_{15/2}$		$^2G_{9/2} \rightarrow {}^4I_{15/2}$	
Center (cm^{-1})	Area	Center (cm^{-1})	Area	Center (cm^{-1})	Area	Center (cm^{-1})	Area
14609	12	17705	13	18522	18	23839	13
14690	5	17727	21	18546	25	23959	4
14768	10	17806	12	18671	4	24025	4
14824	3	17953	6	18701	2	24081	7
14850	2	18042	20	18771	4	24188	5
14928	4	18133	8	18866	3	24260	1
14951	3	18170	3	18892	1	24300	22
15029	11	18216	9	18944	8	24372	6
15071	1	18261	4	18978	6	24422	8
15107	17	18299	2	19017	4	24450	25
15152	6			19048	1	24498	5
15187	5			19078	4	24583	1
15235	4			19125	16		
15270	10			19181	2		
15323	5			19221	2		
15387	1						
15423	1						

The accuracy for establishing individual levels is around 5 cm^{-1}, but, for estimating their combined weight center, a simple arithmetic average was performed, which is a coarse evaluation used for economy. The results are listed in Table 2.

Table 2

Average estimated energy values (cm^{-1}) of the Stark levels for Er^{3+} ion in the Y_2O_3 matrix involved in the upconversion process (individual levels are +/- 5 cm^{-1})

$^4F_{9/2}$	$^4S_{3/2}$	$^2H_{11/2}$	$^2G_{9/2}$	$^4I_{15/2}$
15184	18049	18978	23841	290
15032	17658	18921	23949	238
14773		18789	24008	205
14747		18772	24263	156
14533		18548	24294	119
		18482		76
				38
				0
14854	**17853**	**18748**	**24071**	

Further refinements considering the intensities and the local symmetry group of embedding for the Er^{3+} ions, as well the separation between electric and magnetic dipole transitions should be performed, but these necessitate separate attention which is beyond the scope of present work. Using the average values for the unsplit energy levels involved in the upconversion process, simulations were done for the free Er^{3+} ion by adjusting the free atomic parameters until the deviations of the simulated values from the experimental ones were those from Table 3. It should be mentioned that the granularity of the parameter space is high, and care must be taken in the initialization phase; nevertheless, the convergence is relatively fast (around 50 steps).

Table 3

Atomic parameters used for simulating the energy levels of Er^{3+} ion in the Y_2O_3 matrix (*left*) and deviations (cm^{-1}) from the experimental values for the specified energy levels (*right*).

E_{avg}	-34947.0	T_2	404.0
F_2	95544.0	T_3	42.1
F_4	65834.6	T_4	79.7
F_6	56246.0	T_6	-293.1
ζ	2362.0	T_7	291.1
α	17.7	T_8	267.4
β	-589.8	M_0	3.8
γ	1770.7	P_2	612.0

level	dev(cm^{-1})
$^4F_{9/2}$	2
$^4S_{3/2}$	-2
$^2H_{11/2}$	2
$^2G_{9/2}$	-1

Table 3 lists the chosen atomic parameter values and Table 4 shows the first 17 energy levels resulting from the simulation. The first four most important weights of the respective wavefunctions (Wgt) and their sum (W_{sum}) are provided (Table 4), being an estimation of the richness of the degeneracy of the respective level. Two observations can be made at first glance:

(i) A comparison with the literature data [1,2,18] shows that the energies determined in this work are lower, but the order of the levels is the same. This

discrepancy needs some further investigation since the measurements we have performed on other types of host matrix oxides are highly consistent with that for Y_2O_3, only the strength of the crystal field (and subsequently the widths of the splittings) being different.

(ii) The strong mixing of J manifolds and the low uniformity of the degeneracy for the ground level ($^4I_{15/2}$), is contrary to the richness of the PL spectra, which implies that the simulation model is limited (or needs more input data). Also, the convention for labeling the levels can be misleading (e.g., the stronger component of $^4F_{9/2}$ at the 11th level which is usually labeled $^2G_{9/2}$).

Table 4

Simulated energy levels (cm^{-1}) and partial wavefunction compositions of free Er^{3+} ion which match the cases for $^4F_{9/2}$, $^4S_{3/2}$, $^2H_{11/2}$, $^2G_{9/2}$ experimental estimated levels

Nr	Energy	W_{sum}	Wgt	$LSJM_J$	Wgt	$LSJM_J$	Wgt	$LSJM_J$	Wgt	$LSJM_J$
1	0	0.97	0.74	4I 15/2 11/2	0.13	4I 15/2 7/2	0.08	4I 15/2 -13/2	0.02	2K 15/2 11/2
2	6481	0.82	0.40	4I 13/2 9/2	0.16	4I 13/2 5/2	0.14	4I 13/2 13/2	0.12	4I 13/2 3/2
3	10074	0.63	0.23	4I 11/2 1/2	0.16	4I 11/2 11/2	0.14	4I 11/2 3/2	0.10	4I 11/2 -7/2
4	12168	0.60	0.31	4I 9/2 1/2	0.11	4F 9/2 1/2	0.11	2H2 9/2 1/2	0.06	2G 9/2 1/2
5	14856	0.61	0.19	4F 9/2 -5/2	0.19	4F 9/2 5/2	0.12	4F 9/2 -3/2	0.11	4I 9/2 -5/2
6	17851	0.88	0.58	4S 3/2 -1/2	0.15	2P 3/2 -1/2	0.08	4S 3/2 3/2	0.06	2D 3/2 -1/2
7	18750	0.58	0.23	2H2 11/2 11/2	0.21	4G 11/2 11/2	0.08	4I 11/2 11/2	0.06	2H2 11/2 7/2
8	19927	0.86	0.43	4F 7/2 3/2	0.30	4F 7/2 -1/2	0.07	4F 7/2 1/2	0.06	4F 7/2 7/2
9	21637	0.91	0.56	4F 5/2 -1/2	0.20	4F 5/2 3/2	0.08	2D 5/2 -1/2	0.07	4F 5/2 5/2
10	21924	0.99	0.62	4F 3/2 -3/2	0.21	2D 3/2 -3/2	0.16	4S 3/2 -3/2		
11	24070	0.33	0.11	4F 9/2 9/2	0.09	2G 9/2 9/2	0.07	2G2 9/2 9/2	0.06	2H2 9/2 9/2
12	25755	0.81	0.44	4G 11/2 9/2	0.24	2H2 11/2 9/2	0.09	2H 11/2 9/2	0.04	4G 11/2 5/2
13	26655	0.80	0.38	4G 9/2 3/2	0.22	4G 9/2 -3/2	0.12	4G 9/2 -7/2	0.07	2H2 9/2 3/2
14	27272	0.84	0.55	2K 15/2 -13/2	0.20	2K 15/2 11/2	0.06	2K 15/2 5/2	0.04	2K 15/2 -5/2
15	27298	0.95	0.45	4G 7/2 -7/2	0.24	2G 7/2 -7/2	0.23	2G2 7/2 -7/2	0.04	4F 7/2 -7/2
16	30864	0.82	0.31	2P 3/2 1/2	0.22	4F 3/2 1/2	0.19	2D 3/2 1/2	0.10	4S 3/2 1/2
17	32398	0.87	0.50	4G 5/2 -3/2	0.22	4G 5/2 1/2	0.10	4G 5/2 3/2	0.05	4G 5/2 -5/2

3.4 The efficiency of the upconversion

One can observe that the Yb^{3+} ions presence strongly influences the efficiency of the upconversion process (visible red and green regions) with a sharp increase in the case of YO1-2 relative to YO1-0 and reaching 8.3 times higher in the case of YO1-4 than for YO1-0 sample, in which the sensitizer Yb^{3+} ions are not present. Increasing the Yb^{3+} ions concentration leads to quenching effects and therefore, for YO1-8, the total luminesce intensity in the visible domain is lower than that of YO1-4 ceramic.

Nevertheless, when the Yb^{3+} sensitizer ions are present, the total (red+green) efficiencies are comparable, but the red/green intensities ratio is changing almost linearly with the logarithm of the Yb^{3+} concentrations, as can be seen in Fig. 16 (right), the red emission being promoted, which means that, in the presence of Yb^{3+} ions, the populating of $^4F_{9/2}$ level is more probable than that of

$^4S_{3/2}$ level. This linear variation can be linked to the decrease of the relative interionic distance between Er^{3+} and Yb^{3+} neighbors as can be observed in Fig. 17.

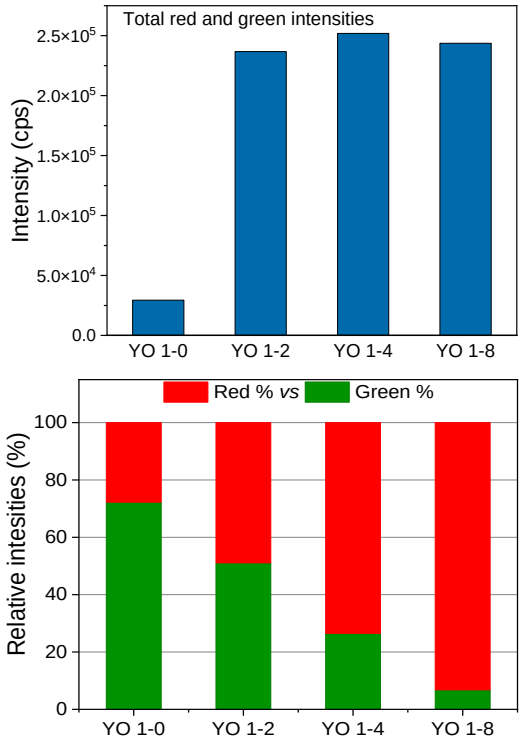

Fig. 16 - Intensity (in counts) of the luminescence (RED and GREEN emission) for Y_2O_3:Er,Yb phosphors *(left)* and the percentile *relative* intensities of the RED versus GREEN emissions for Y_2O_3:Er,Yb phosphors *(right.)*

The distributions of interionic distance from the nearest 1, 4, 6 and 8 Yb^{3+} neighbors surrounding an Er^{3+} ion, to it, simulated for an Y_2O_3 cubic crystal with an edge length of 330 nm, are Poissonian and their peak values are indicated in Table 5. For YO1-8 more than 40% of the Yb^{3+} ions are at a distance of 3.5 Å from the nearest Er^{3+} ion, i.e. are among the closest neighbors for the Er^{3+} ions.

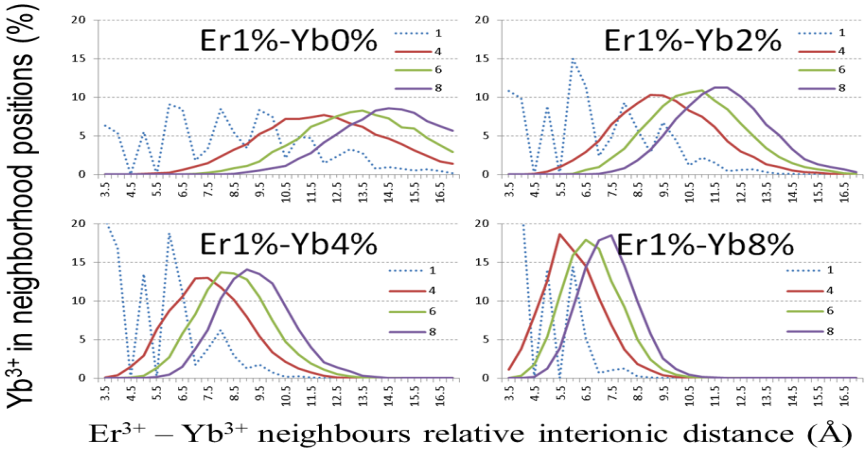

Fig. 17 - Distributions of the average distances from the nearest 1, 4, 6, 8 Yb^{3+} neighbours surrounding an Er^{3+} ion, to it, simulated for an Y_2O_3 cubic crystal with the edge length of 330 nm.

3.5. Proposed upconversion mechanism

The analysis of the visible upconversion spectra has shown that the total intensity (red and green) is highest in the case of YO1-4. When Yb^{3+} is not present, the native Er^{3+} upconversion is weak and mostly in the green part.

Table 5

Peak values (Å) for the distributions shown in Fig. 17 of Yb^{3+} neighboring ions around an Er^{3+} ion

Neighbours	n=4	n=6	n=8
YO 1-0	11.7	13.3	14.2
YO 1-2	9.2	10.7	11.7
YO 1-4	7.3	8.3	9.2
YO 1-8	5.8	6.6	7.3

The Yb^{3+} ions presence strongly influences the upconversion process, and when the concentration of Yb^{3+} is 8%, the intensity of red emission is the highest.

The observation that the relative ratio of red versus green emissions is linearly correlated with the logarithm of the Yb^{3+} versus Er^{3+} concentrations ratio, underlines that the presence of Yb^{3+}, when more closely surrounding Er^{3+}, enhances the population of $^4F_{9/2}$ level either through a virtual one located between $^4F_{9/2}$ and $^4S_{3/2}$ (from which the decay to $^4F_{9/2}$ level is performed via phononic channels) or through a quick direct decay from $^4S_{3/2}$ to $^4F_{9/2}$.

Because the $^4F_{9/2}$ level of Er^{3+} is strongly populated in the presence of Yb^{3+}, the probability of absorbing the incident NIR radiation and transitioning to $^2G_{9/2}$ level (also through a virtual one) is increased, and the decay to ground state ($^4I_{15/2}$)

generates the 415 nm line. Fig. 18 depicts a plausible mechanism based on the experimental results.

4. Conclusions

Pellets of yttria ceramic doped with Er^{3+} and Yb^{3+} ions in various relative ratios and absolute percentages were sintered at 1300°C from the corresponding powders prepared by coprecipitation route, which was found as a suitable method for RE ions accommodation in the crystalline cubic lattice of the Y_2O_3 host matrix. Y_2O_3:Er,Yb ceramics were used to study the upconversion process of the incident NIR irradiation of 976 nm by Er^{3+} ions sensitized by Yb^{3+} ions and an upconversion mechanism was proposed. Nevertheless, for higher precision, the crystal field strength that leads to the splitting of the Stark levels will be determined in future work.

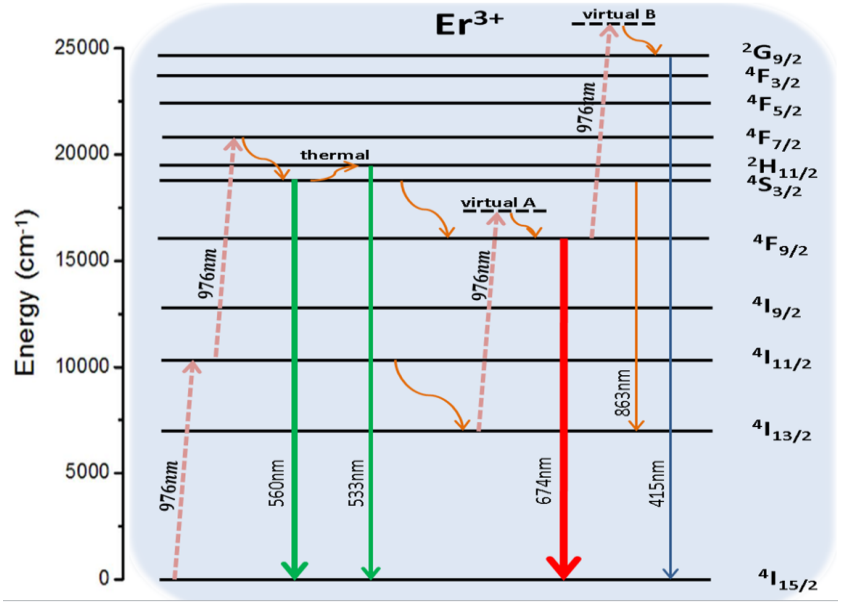

Fig. 18 - An alleged scheme for the transitions involved in the upconversion mechanism. Curved arrows indicate transitions that can involve phononic energy transfers.

REFERENCES

1. Freidzon, A. Ya., Kurbatov, I.A., Vovna, V.I. Ab initio calculation of energy levels of trivalent lanthanide ions, Phys. Chem. Chem. Phys. **(2018)**, 20, 14564-14577, DOI: 10.1039/C7CP08366A.

2. Morrison, C.A. and Leavitt, R.P., Spectroscopic Properties of Triply Ionized Lanthanides in Transparent Host Crystals, Handbook on the Physics and Chemistry of Rare Earths, Editors K.A. Gschneidner, Jr. and L. Eyring, North-Holland Publishing Co. (**1982**).
3. Forest, H. and Ban, G. Evidence for Eu^{+3} Emission from Two Symmetry Sites in $Y_2O_3:Eu^{+3}$, J. Electrochem. Soc. **1969**, 116**,** 474, DOI 10.1149/1.2411909.
4. G. Schnaack, J. A. Konigstein, Phonon and Electron Raman Spectra of Cubic Rare-Earth Oxides and Isomorphous Yttrium Oxide, J. Opt. Soc. Am., (**1970)**, 60, 1110-1115 doi 10.1364/JOSA.60.001110.
5. Wen, S., Zhou, J., Zheng, K., Bednarkiewicz, A., Liu X. Jin, D., Advances in highly doped upconversion nanoparticles. Nature Commun. (**2018),** 9, 2415, doi:10.1038/s41467-018-04813-5
6. Feuk, H. Nilsson S., Richter, M., Upconversion phosphor thermometry for use in thermal barrier coatings, Meas. Sci. Technol. (**2023),** 34, 064003.
7. Yang, L., Fu, Y., Cheng, W., Peng, D., Chen, Z., Luo, L., Zhao, X., Liu, Y., Kou, Z. Europium and erbium co-doped yttria-stabilized zirconia as a potential dual-sensor for simultaneous oxygen partial pressure and temperature measurements. Ceram. Int. (**2023),** 49, 10961–10975.
8. Yang, X., Liu, M., Liu, J., Xia, Y., Ji, W., Li, Z, Chen, J., Liu, L., Hao, L., Dong, B., Agathopoulos, S., Xu, X. Mechanism of upconversion luminescence enhancement in Yb^{3+}/Er^{3+} co-doped Y_2O_3 through Li^+ incorporation. Phys. Chem. Chem. Phys. (**2020)**, 22, 2819-2826, DOI: 10.1039/C9CP06137A.
9. Wang, N., Zhang, X., Bai, Z. Fabrication of highly transparent Er^{3+}, Yb^{3+}:Y_2O_3 ceramics with La_2O_3/ZrO_2 as sintering additives and the near-infrared and upconversion luminescence properties. J. Alloys Comp. (**2020)**, 842, 155932, doi.org/10.1016/j.jallcom.2020.155932.
10. Zhao, J.B., Wu, L., Yb^{3+}- and Er^{3+}-doped Y_2O_3 microcrystals for upconversion photoluminescence and energy transfer with enhancements of near-ultraviolet emission, Rare Metals (**2021),** 40, 123–127, DOI: 10.1007/s12598-019-01269-4.
11. Tabanli, S., Eryurek G. Upconversion luminescence properties of Y_2O_3: $Yb^{3+}/Er^{3+}/Tm^{3+}$ nanocrystal doped PMMA nanocomposites, J. Non-Crystalline Solids (**2019),** 505, 43-51, https://doi.org/10.1016/j.jnoncrysol.2018.10.041.
12. Xie, N., Pei, M., Ming, C., Strong upconversion emissions in Er^{3+} doped Y_2O_3 nanocrystals prepared using a 'PMMA-polymerization route, Optik (**2018)**, 174, 125-128, https://doi.org/10.1016/j. ijleo.2018.08.045.
13. Moorthy, L.R., Srinivasa Rao, T., Janardhnam, K., Radhapathy, A., Absorption and emission characteristics of Er^{3+} ions in alkali chloroborophosphate glasses, Spectrochim. Acta Part A (**2000)**, 56 1759–1771, doi.org/10.1016/S1386-1425(00)00234-1
14. C.K. Jørgensen, Modern Aspects of Ligand Field Theory, North-Holland, Amsterdam, (**1971**) doi.org/10.1002/bbpc.19710751033.
15. F. Auzel, O.L. Malta, A scalar crystal field strength parameter for rare-earth ions: meaning and usefulness J. Phys. **(1983),** 44, 201-206 DOI: 10.1051/jphys:01983004402020100.
16. Malta, O. L., Antic-Fidancev, E., Lemaitre-Blaise, M., Milicic-Tang, A., Taibi, M. The crystal field strength parameter and the maximum splitting of the $^7F_1$ manifold of the Eu^{3+} ion in oxides, J. Alloys Comp. 228, (**1995)**, 41 doi.org/10.1016/0925-8388(95)01645-7.

17. Momma, K. and Izumi, F. VESTA 3 for three-dimensional visualization of crystal, volumetric and morphology data, J. Appl. Crystallogr., (**2011)**, 44, 1272-1276.
18. Radžiūtė, L., Gaigalas, G., Kato, D., Jönsson, P., Rynkun, P., Kučas, S., Jonauskas, V., Matulianec, R., Energy level structure of Er^{3+}, J. Quant. Spectros. & Radiative Transfer (**2015)**, 152, 94–106 doi.org/10.1016/j.jqsrt.2014.11.007.